

# Spontaneous fission half-life in Fm isotopes with nuclear energy density functional

Kouhei Washiyama<sup>1,\*</sup>

<sup>1</sup>Center for Computational Sciences, University of Tsukuba, Tsukuba, 305-8577, Japan

**Abstract.** A microscopic description of fission dynamics is important to understand the decay properties of neutron-rich heavy nuclei that are relevant to  $r$ -process nucleosynthesis. To provide a reliable and efficient method to evaluate the spontaneous fission half-life, we develop a method, called the constrained Hartree–Fock–Bogoliubov (CHFb) plus local quasiparticle random-phase approximation (LQRPA), to include dynamical residual effects in the collective inertia. With the CHFb + LQRPA, we evaluate the collective potential and the collective inertia along a mass-symmetric fission path in Fm isotopes with the neutron numbers  $N = 158–164$ . The obtained LQRPA inertia is much larger than the cranking one that ignores dynamical residual effects and shows a remarkable variation along the fission path. We estimate the fission half-life of the Fm isotopes using the action integral with the obtained collective potential and inertia. A large difference between the fission half-lives obtained with the LQRPA inertia and with the cranking inertia is observed. This indicates the importance of evaluating the collective inertia for estimating the fission half-life.

## 1 Introduction

Nuclear fission attracts much interest in various subjects [1]. One of the recent applications on fission is the nuclear reaction network calculations of the  $r$ -process nucleosynthesis simulations [2, 3] since low-energy fission in the  $r$ -process environment may determine the end point of the  $r$ -process nucleosynthesis and a part of the abundance patterns of the elements in the universe. The network calculations involve experimentally unknown nuclei. Therefore, a microscopic model for fission is necessary to describe fission dynamics of both stable and unstable nuclei [4].

The nuclear energy density functional (EDF) theory has been widely used for various objectives in nuclear physics as a microscopic model. The nuclear EDF gives a good description of the ground-state property of nuclei in the whole nuclear chart [5, 6]. Recently, a microscopic description for fission has been developed with EDF approaches [7–14]. In these EDF approaches, spontaneous or low-energy fission has been described with the Wenzel–Kramers–Brillouin (WKB) approximation for quantum many-body tunneling. The potential energy and the collective inertia used in the WKB approximation have been calculated with the constrained Hartree–Fock–Bogoliubov (HFb) method with constraint on the collective variables and with the so-called cranking approximation [15, 16], respectively. It is well known that the cranking approximation ignores dynamical residual effects, particularly time-odd terms of the EDF, in the collective inertia. This gives a significant deviation from the collective inertia that includes the dynamical residual effects [17]. However, the

cranking approximation has been widely used because of its low computational cost.

In a microscopic derivation of the five-dimensional quadrupole collective Hamiltonian [18], the constrained HFb (CHFb) plus local quasiparticle random-phase approximation (LQRPA) [19] was proposed to properly include the dynamical residual effects in the inertial functions. The CHFb + LQRPA has been applied to the construction of the collective Hamiltonian in triaxial shapes with the semi-realistic pairing-plus-quadrupole Hamiltonian [19–23]. To limit axially symmetric shapes, the collective Hamiltonian was constructed with the Skyrme EDF [24].

Recently, we applied the CHFb + LQRPA method with the Skyrme EDF to the description of the collective inertia along the mass-symmetric fission path and showed the importance of the improved collective inertia in the description of the fission dynamics [25]. To overcome a problem of high computational cost to evaluate the collective inertia with the LQRPA, we employed the finite amplitude method (FAM) [26–28]. In this paper, we extend this work to the description of the fission half-life in Fm isotopes.

## 2 Method

Since the formulation of the CHFb + LQRPA for the collective inertia along the fission path was presented in Refs. [19, 25], we give in this section a brief explanation of the formulation. Here, we assume one collective coordinate  $q$  to describe the fission dynamics.

\*e-mail: washiyama@nucl.ph.tsukuba.ac.jp

The collective potential is obtained by solving the CHFB equation with a given constraining operator  $\hat{s}$ ,

$$\delta\langle\phi(s)|\hat{H}_{\text{CHFB}}|\phi(s)\rangle = 0, \quad (1)$$

$$\hat{H}_{\text{CHFB}} = \hat{H}_{\text{HFB}} - \sum_{\tau=n,p} \lambda_{\tau} \hat{N}_{\tau} - \lambda_s \hat{s}, \quad (2)$$

where  $\lambda_{n,p}$  and  $\hat{N}_{n,p}$  denote the Fermi energies and the number operators, respectively, for neutrons and protons, and  $\lambda_s$  is a Lagrange multiplier of constraining the collective variable  $s = \langle\phi(s)|\hat{s}|\phi(s)\rangle$ . The energy minimization in Eq. (1) leads to the CHFB state  $|\phi(s)\rangle$  and collective potential  $V(s) = \langle\phi(s)|\hat{H}_{\text{HFB}}|\phi(s)\rangle$ .

The collective inertia is determined by local normal modes build on CHFB states. On top of the CHFB state  $|\phi(s)\rangle$ , the LQRPA equations,

$$\delta\langle\phi(s)|[\hat{H}_{\text{HFB}}, \hat{Q}_i(s)] - \frac{1}{i} \hat{P}_i(s)|\phi(s)\rangle = 0, \quad (3)$$

$$\delta\langle\phi(s)|[\hat{H}_{\text{HFB}}, \frac{1}{i} \hat{P}_i(s)] - \Omega_i^2(s) \hat{Q}_i(s)|\phi(s)\rangle = 0, \quad (4)$$

are solved to determine the local generators  $\hat{Q}_i(s)$  and  $\hat{P}_i(s)$  defined at  $s$ . Here,  $\Omega_i^2(s)$  is the squared eigen-frequency of the local normal mode. Once the local normal mode is selected, the collective kinetic energy is expressed in terms of the collective variable  $s$  as [19]

$$T = \frac{1}{2} \dot{q}^2 = \frac{1}{2} \mathcal{M}(s) \dot{s}^2, \quad (5)$$

where the collective inertia  $\mathcal{M}(s)$  is defined as

$$\mathcal{M}(s) = \frac{dq}{ds} \frac{dq}{ds}. \quad (6)$$

The inverse of the derivative is evaluated using the local generator  $\hat{P}_i(s)$  as

$$\frac{ds}{dq} = \frac{d}{dq} \langle\phi(s)|\hat{s}|\phi(s)\rangle = \langle\phi(s)|[\hat{s}, \frac{1}{i} \hat{P}_i(s)]|\phi(s)\rangle. \quad (7)$$

Thus, the collective inertia (6) is determined by the local normal mode of the LQRPA equations. Note that the above formulation can be generalized to the cases with more than one collective coordinates [19].

As a constrained operator to describe the coordinate of the mass-symmetric fission path, the axially symmetric mass quadrupole operator,

$$\hat{s} = \hat{Q}_{20} = \sqrt{\frac{16\pi}{5}} \sum_{i=1}^A r_i^2 Y_{20}(\hat{r}_i), \quad (8)$$

is used. To limit axially symmetric shapes, the triaxiality  $\langle\hat{Q}_{22}\rangle = 0$  is kept, which is defined as  $\hat{Q}_{22} = \sqrt{16\pi/5} \sum_{i=1}^A r_i^2 [Y_{22}(\hat{r}_i) + Y_{2-2}(\hat{r}_i)] / \sqrt{2}$ . For the potential energy, we solve the CHFB equation with the two-basis method [29, 30] in a three-dimensional Cartesian mesh. Enforcing the reflection symmetries about the  $x = 0$ ,  $y = 0$ , and  $z = 0$  planes, we use a numerical box of  $11.5 \text{ fm} \times 11.5 \text{ fm} \times 16.5 \text{ fm}$  in  $x > 0$ ,  $y > 0$ ,  $z > 0$  with a mesh size of  $1.0 \text{ fm}$ . With these reflection symmetries, odd multipole moments (e.g., octupole moments)

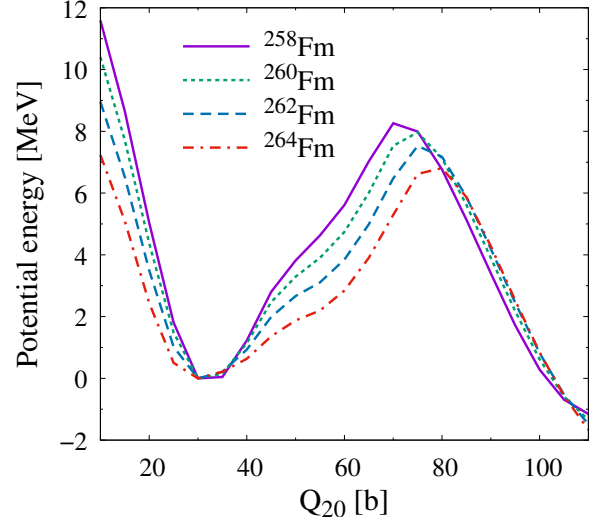


**Figure 1.** Collective potential energy as a function of  $Q_{20}$  for Fm isotopes calculated with the CHFB. The solid, dotted, dashed, and dot-dashed lines denote the results of  $^{258}\text{Fm}$ ,  $^{260}\text{Fm}$ ,  $^{262}\text{Fm}$ , and  $^{264}\text{Fm}$ , respectively. The collective potential energy is shifted so as to make its minimum energy zero.

can not be considered. Namely, mass-asymmetric fission paths are not in the present scope. The single-particle basis consists of 1820 neutron and 1440 proton Hartree-Fock basis states to achieve the maximum quasiparticle energy  $E_{\text{QP}}^{\text{max}} \approx 60 \text{ MeV}$ . For the CHFB + LQRPA calculations, we follow Ref. [25] and use the FAM [26–28], in particular the FAM with contour integration technique developed in Ref. [31], for the solution of the LQRPA equations. We choose the most collective mode among LQRPA modes in low frequencies  $\Omega_i^2 < 16 \text{ MeV}^2$  following the prescription in Ref. [25]. We solve the CHFB + LQRPA in  $Q_{20} = \langle\hat{Q}_{20}\rangle \leq 110 \text{ b}$  with  $\Delta Q_{20} = 5 \text{ b}$ . We used the SkM\* EDF [32] and the contact volume pairing with a pairing window of  $20 \text{ MeV}$  described in Ref. [33]. The pairing strengths were adjusted separately for neutrons and protons to reproduce the empirical pairing gaps in  $^{256}\text{Fm}$ .

### 3 Results and Discussions

We show the results of the mass-symmetric fission for the even-even Fm isotopes with the neutron numbers  $N = 158\text{--}164$ . The reason why we chose  $^{258,260,262,264}\text{Fm}$  is that the mass distributions of fission fragments in  $^{258,259}\text{Fm}$  are symmetric and experimental systematic observation in the mass region around Fm isotopes suggests the mass-symmetric fission in Fm isotopes with  $N \geq 158$  [34]. We did not investigate odd- $N$  Fm isotopes because of difficulty to handle odd nuclei in the present EDF framework.

#### 3.1 Collective potential and pairing gaps

First, we show the collective potentials of the Fm isotopes calculated with the CHFB method along the mass-symmetric fission path. Figure 1 shows the collective potential as a function of  $Q_{20}$  for  $^{258,260,262,264}\text{Fm}$ . The ob-

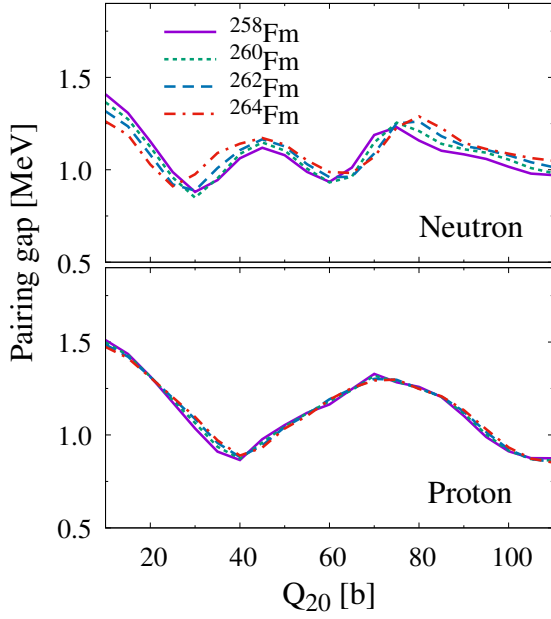


**Figure 2.** Neutron (top) and proton (bottom) pairing gaps as a function of  $Q_{20}$  for the Fm isotopes.

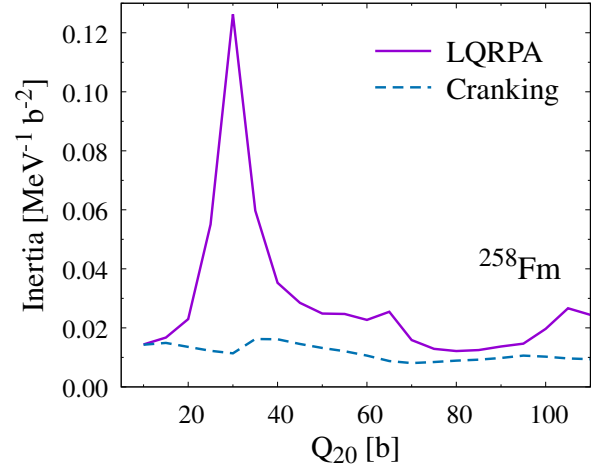
tained potential energies are shifted so as to make the minimum energy of each nucleus set to be zero. The collective potential shows a neutron-number dependence and as the neutron number increases, the fission barrier height decreases and the value of  $Q_{20}$  at the barrier position increases. The value of  $Q_{20}$  at the minimum energy is similar to each other. In each nucleus, the energy becomes negative at  $Q_{20} \geq 105$  b.

Figure 2 shows the neutron and proton pairing gaps in the Fm isotopes. In neutron, the variation of the gap on  $Q_{20}$  is similar to each other. In the proton gaps, almost the same  $Q_{20}$  dependence is obtained among different Fm isotopes.

### 3.2 Collective inertia

Next, we discuss the collective inertia along the fission path in the Fm isotopes. Figure 3 shows the collective inertia obtained with the CHF + LQRPA method denoted as the solid line as a function of  $Q_{20}$  for  $^{258}\text{Fm}$ . A sharp increase at  $Q_{20} \approx 30$  b, where the ground state is located, is seen. A similar structure to this was presented in  $^{240}\text{Pu}$  and  $^{256}\text{Fm}$  in Ref. [25]. In Fig. 3, the collective inertia with the perturbative cranking approximation that ignores the dynamical residual effects is shown by the dashed line. At all  $Q_{20}$ , the LQRPA inertia is larger than the cranking one, and a variation of the LQRPA inertia is remarkable. The dynamical residual effects significantly increase the collective inertia.

Figure 4 shows the LQRPA collective inertia for the Fm isotopes. The collective inertia for all the isotopes has similar  $Q_{20}$  dependence: a sharp increase at  $Q_{20} \approx 30$  b and smooth behavior around  $Q_{20} \approx 80$  b, at the top of the fission barrier.



**Figure 3.** Collective inertia as a function of  $Q_{20}$  for  $^{258}\text{Fm}$ . The solid and dashed lines correspond to the collective inertia obtained with the LQRPA and the one with the perturbative cranking approximation, respectively.

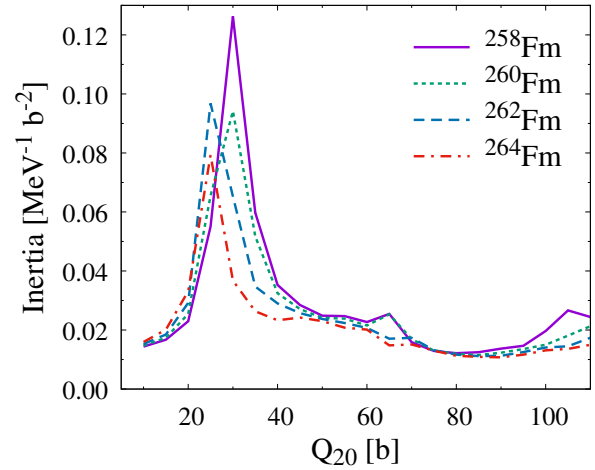


**Figure 4.** Collective inertia obtained with the CHF + LQRPA method for different Fm isotopes.

### 3.3 Spontaneous fission half-life

From the collective potential and the collective inertia along the fission path, the spontaneous fission half-life can be estimated. The fission half-life is given by

$$T_{1/2} = \ln 2 / (nP), \quad (9)$$

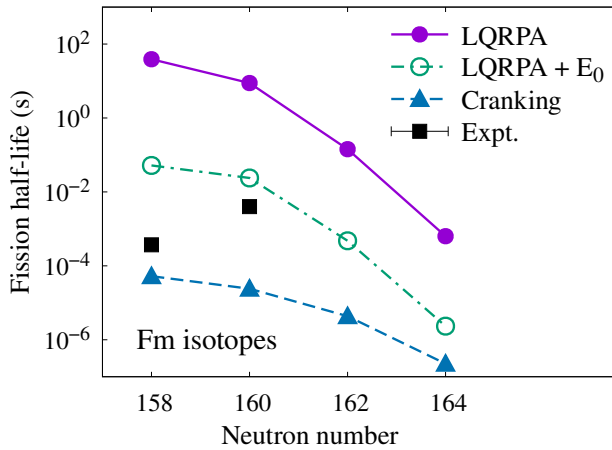
where  $n$  is the number of assaults on the fission barrier per unit time. According to the former works [13],  $n = 10^{20.38} \text{ s}^{-1}$  is employed.  $P$  denotes the penetrability given as

$$P = [1 + \exp(2S)]^{-1}, \quad (10)$$

where the action  $S$  is given in the WKB approximation as

$$S = \int_{Q_{\text{in}}}^{Q_{\text{out}}} dQ_{20} \sqrt{2\mathcal{M}(Q_{20})[V(Q_{20}) - E_0]}, \quad (11)$$

where  $Q_{\text{in}}$  and  $Q_{\text{out}}$  are the classical inner and outer turning points along the fission path, respectively, and  $E_0$  denotes the ground-state energy.



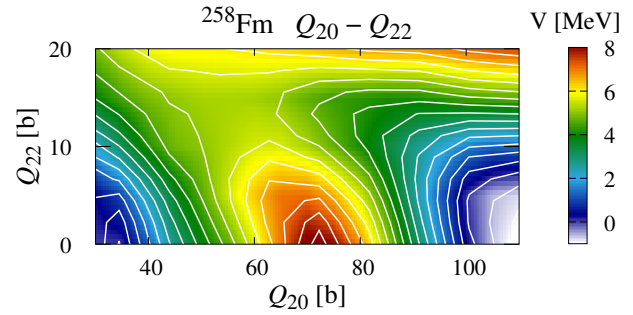
**Figure 5.** Spontaneous fission half-life obtained with the LQRPA inertia by the filled-circle solid line and with the cranking inertia by the filled-triangle dashed line for the Fm isotopes, compared with the experimental data [35] by the filled squares. The open-circle dot-dashed line shows the result of the LQRPA inertia by adding a zero-point energy correction of  $E_0 = 0.5$  MeV (see text).

Figure 5 shows the spontaneous fission half-life obtained with the LQRPA inertia (filled-circle solid line) and with the cranking inertia (filled-triangle dashed line) in the Fm isotopes. In these results, the ground-state energy is set  $E_0 = 0$ . The available experimental data are plotted by squares [35]. Note that the experimental data point for  $^{260}\text{Fm}$  may be questionable, see the NUBASE2020 evaluation [36] for detail. The fission half-life obtained with the LQRPA inertia is 4–6 orders of magnitude larger than that with the cranking inertia. This difference originates from only the difference in the collective inertia with or without the dynamical residual effects. The fission half-life is significantly sensitive to the choice of the collective inertia. The fission half-lives obtained with both the LQRPA inertia and cranking one decrease as the neutron number increases, which is expected from the collective potential and the collective inertia. The spontaneous fission half-life with the LQRPA inertia deviates from the experimental one by several orders of magnitude.

### 3.4 Discussions

The significant deviation between the fission half-life in the theory and experimental one indicates a room for the improvement of the theory. To improve the description of the fission half-life, the following points can be considered.

First point is to consider zero-point energy corrections to the ground-state energy  $E_0$  and/or to the collective potential energy in the action in Eq. (11). In some of former works [9, 12–14], a constant value has been employed for the ground-state energy  $E_0$  and/or the vibrational and rotational zero-point energy corrections to the collective potential energy have been considered by using the Gaussian overlap approximation to the generator-coordinate method. In this paper, we tested a constant value for the



**Figure 6.** Potential energy surface in the  $Q_{20}$ – $Q_{22}$  plane for  $^{258}\text{Fm}$ . The minimum energy is set to be zero. The contour interval is 0.5 MeV.

ground-state energy of  $E_0 = 0.5$  MeV. The result is shown by the open-circle dot-dashed line in Fig. 5, denoted as LQRPA +  $E_0$ . This simple correction in the ground-state energy decreases the fission half-life in about 3 orders of magnitude. It is however noticed that the description of the zero-point energy correction should be consistent with the estimation of the number of assaults  $n$  in Eq. (9) and further considerations are necessary.

Second point is to take more than one collective variable into account for fission dynamics. Former works showed that inclusion of triaxial shapes reduces the fission barrier height by a few MeV in Fm isotopes [7, 9, 10]. This reduction is expected to give a decrease in the action  $S$ , and decrease in the fission half-life. Figure 6 shows the potential energy surface as functions of  $Q_{20}$  and triaxiality  $Q_{22}$  calculated with the CHFb with the SkM\* EDF for  $^{258}\text{Fm}$ . One clearly sees that the height of the fission barrier is reduced by about 3 MeV by including triaxial deformations with  $Q_{22} > 0$ . Then, the fission path that corresponds to the minimized potential changes from the axially symmetric shape to triaxial shapes. It is noticed that since the collective inertia obtained with the CHFb + LQRPA much more strongly depends on the collective variables than the cranking inertia does, the least-action path in Eq. (11) might be different from the path that corresponds to the minimized potential. This will affect the description of the fission half-life.

## 4 Summary

In this paper, we investigated the fission half-lives in the even–even Fm isotopes with  $N = 158$ – $164$ , in which the mass-symmetric fission mode is expected to be dominant. We performed the CHFb + LQRPA calculations to obtain the collective potential and inertia along the fission path and perform the action integral to obtain the fission half-life. We clearly show that the improved description of the collective inertia changes the story of spontaneous fission. Namely, compared with the result obtained with the cranking inertia, the LQRPA inertia becomes significantly larger, and then makes the fission half-life longer. However, a large discrepancy between the fission half-life with the CHFb + LQRPA and experimental one is found. Including the zero-point energy correction and other col-

lective variables than the axially symmetric quadrupole moment  $Q_{20}$  might give a better description of the fission half-life. The work along these lines is in progress.

## Acknowledgments

Numerical calculations were performed using computational resources of Wisteria/BDEC-01 Odyssey (the University of Tokyo), provided by the Multidisciplinary Cooperative Research Program in the Center for Computational Sciences, University of Tsukuba.

## References

- [1] A.N. Andreyev, K. Nishio, K.H. Schmidt, Rep. Prog. Phys. **81**, 016301 (2017)
- [2] M.R. Mumpower, R. Surman, G.C. McLaughlin, A. Aprahamian, Prog. Part. Nucl. Phys. **86**, 86 (2016)
- [3] S.A. Giuliani, G. Martínez-Pinedo, L.M. Robledo, Phys. Rev. C **97**, 034323 (2018)
- [4] M. Bender, R. Bernard, G. Bertsch, S. Chiba, J. Dobaczewski, N. Dubray, S.A. Giuliani, K. Hagino, D. Lacroix, Z. Li et al., J. Phys. G **47**, 113002 (2020)
- [5] M. Bender, P.H. Heenen, P.G. Reinhard, Rev. Mod. Phys. **75**, 121 (2003)
- [6] T. Nakatsukasa, K. Matsuyanagi, M. Matsuo, K. Yabana, Rev. Mod. Phys. **88**, 045004 (2016)
- [7] M. Warda, J.L. Egido, L.M. Robledo, K. Pomorski, Phys. Rev. C **66**, 014310 (2002)
- [8] L. Bonneau, P. Quentin, D. Samsøen, Eur. Phys. J. A **21**, 391 (2004)
- [9] A. Staszczak, A. Baran, J. Dobaczewski, W. Nazarewicz, Phys. Rev. C **80**, 014309 (2009)
- [10] H. Abusara, A.V. Afanasjev, P. Ring, Phys. Rev. C **82**, 044303 (2010)
- [11] A. Baran, J.A. Sheikh, J. Dobaczewski, W. Nazarewicz, A. Staszczak, Phys. Rev. C **84**, 054321 (2011)
- [12] A. Staszczak, A. Baran, W. Nazarewicz, Phys. Rev. C **87**, 024320 (2013)
- [13] J. Sadhukhan, K. Mazurek, A. Baran, J. Dobaczewski, W. Nazarewicz, J.A. Sheikh, Phys. Rev. C **88**, 064314 (2013)
- [14] R. Rodríguez-Guzmán, L.M. Robledo, Phys. Rev. C **89**, 054310 (2014)
- [15] M. Girod, B. Grammaticos, Nucl. Phys. A **330**, 40 (1979)
- [16] P. Ring, P. Schuck, *The Nuclear Many-Body Problem* (Springer-Verlag, New York, 1980)
- [17] J. Dobaczewski, J. Skalski, Nucl. Phys. A **369**, 123 (1981)
- [18] A. Bohr, B.R. Mottelson, *Nuclear Structure* (Benjamin, New York, 1975), Vol. II
- [19] N. Hinohara, K. Sato, T. Nakatsukasa, M. Matsuo, K. Matsuyanagi, Phys. Rev. C **82**, 064313 (2010)
- [20] N. Hinohara, K. Sato, K. Yoshida, T. Nakatsukasa, M. Matsuo, K. Matsuyanagi, Phys. Rev. C **84**, 061302(R) (2011)
- [21] K. Sato, N. Hinohara, Nucl. Phys. A **849**, 53 (2011)
- [22] N. Hinohara, Z.P. Li, T. Nakatsukasa, T. Nikšić, D. Vretenar, Phys. Rev. C **85**, 024323 (2012)
- [23] K. Sato, N. Hinohara, K. Yoshida, T. Nakatsukasa, M. Matsuo, K. Matsuyanagi, Phys. Rev. C **86**, 024316 (2012)
- [24] K. Yoshida, N. Hinohara, Phys. Rev. C **83**, 061302(R) (2011)
- [25] K. Washiyama, N. Hinohara, T. Nakatsukasa, Phys. Rev. C **103**, 014306 (2021)
- [26] T. Nakatsukasa, T. Inakura, K. Yabana, Phys. Rev. C **76**, 024318 (2007)
- [27] T. Inakura, T. Nakatsukasa, K. Yabana, Phys. Rev. C **80**, 044301 (2009)
- [28] P. Avogadro, T. Nakatsukasa, Phys. Rev. C **84**, 014314 (2011)
- [29] B. Gall, P. Bonche, J. Dobaczewski, H. Flocard, P.H. Heenen, Z. Phys. A **348**, 183 (1994)
- [30] J. Terasaki, P.H. Heenen, P. Bonche, J. Dobaczewski, H. Flocard, Nucl. Phys. A **593**, 1 (1995)
- [31] N. Hinohara, M. Kortelainen, W. Nazarewicz, Phys. Rev. C **87**, 064309 (2013)
- [32] J. Bartel, P. Quentin, M. Brack, C. Guet, H.B. Håkansson, Nucl. Phys. A **386**, 79 (1982)
- [33] W. Ryssens, V. Hellemans, M. Bender, P.H. Heenen, Comput. Phys. Commun. **187**, 175 (2015)
- [34] M.R. Lane, K.E. Gregorich, D.M. Lee, M.F. Mohar, M. Hsu, C.D. Kacher, B. Kadkhodayan, M.P. Neu, N.J. Stoyer, E.R. Sylwester et al., Phys. Rev. C **53**, 2893 (1996)
- [35] N.E. Holden, D.C. Hoffman, Pure and Applied Chemistry **72**, 1525 (2000)
- [36] F. Kondev, M. Wang, W. Huang, S. Naimi, G. Audi, Chinese Physics C **45**, 030001 (2021)